



Failure analysis of an MVR (mechanical vapor recompressor) Impeller

Keith Alexander^a, Brian Donohue^a, Troy Feese^b, Gordon Vanderlinden^c, Milo Kral^{a,*}

^a Department of Mechanical Engineering, University of Canterbury, Christchurch, New Zealand

^b Engineering Dynamics Incorporated, San Antonio, TX, USA

^c Opus International Consultants, PO Box 1482, Christchurch 8140, New Zealand

ARTICLE INFO

Article history:

Received 29 January 2010

Received in revised form 29 March 2010

Accepted 29 March 2010

Available online 2 April 2010

Keywords:

Impeller failures

Fatigue

Torsional vibration

Variable speed drive

ABSTRACT

This article describes the root cause failure analysis of a mechanical vapor recompressor (MVR) impeller used in a dairy processing plant. An impeller blade was thrown during commissioning after approximately 150 h of service. Visual examination of the blade's fracture surface indicated that the crack growth mechanism was fatigue and this was confirmed by scanning electron microscope (SEM) examinations. A detailed investigation was commissioned to determine the source of the oscillatory stresses that must have been present to cause fatigue. A vibration analysis indicated large torsional oscillatory stresses, leading to fatigue, were induced by excitation of the 1st and 2nd torsional vibration modes of the MVR impeller and motor system. The excitation was induced by the control system for the motor variable speed drive (VSD).

© 2010 Elsevier Ltd. All rights reserved.

1. Introduction

Mechanical vapor recompression (MVR) systems are used to concentrate heat sensitive products (such as food and dairy). The MVR is only one component of many in a complex industrial process. However, a lack of redundancy exists so a catastrophic failure is not only expensive in terms of repair or replacement cost, but also in lost production.

The MVR system consists of an induction motor driving a MVR fan through a coupling as is shown in Fig. 1. The motor speed is controlled by a variable speed drive (VSD). Details are listed below:

Induction motor with four poles: rated 710 kW (952 HP) at 1489 rpm, 415 V, 1160 A.

VSD (variable speed drive): 630 kW (844 HP), 400 V; Pulse Width Modulation (PWM) 4000 Hz Switching frequency; six pulse inverter; Drive Electrical Frequency = 10–71 Hz.

Spacer coupling contains eight buffer bushings and has variable torsional stiffness.

Fan Impeller has 16 full length blades and 16 short blades with an operating speed range from 300 to 2115 rpm.

It is important to note that Pulse Width Modulation drives have varying levels of performance depending on the control algorithms used. In the present case, two different motor control types could easily be used:

1. Voltage/frequency ratio (V/Hz) is an open-loop control and considered the most basic. The speed reference is provided and controls the voltage and frequency applied to the motor. There is no feedback provided for speed so the actual (precise) speed of the motor/fan system is unknown. If load torque changes, which affects the motor slip, the frequency is not

* Corresponding author.

E-mail address: milo.kral@canterbury.ac.nz (M. Kral).

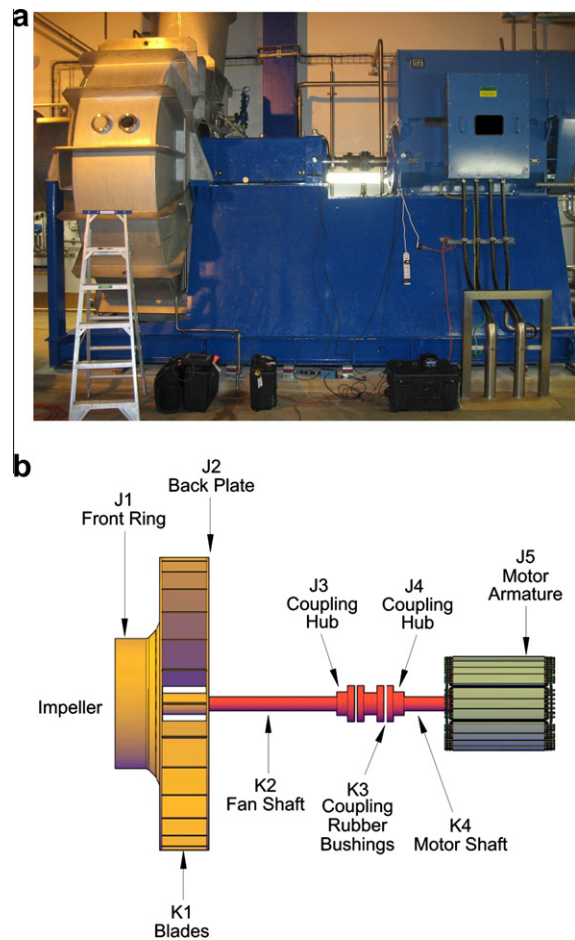


Fig. 1. MVR system and schematic.

compensated so the ratio of V/Hz remains constant. Current is not controlled and only limited if it exceeds the motor or drive rating (typically 150% of full load). This control method is acceptable for simple applications such as centrifugal pumps and fans. This method is not good for motors running at low speeds (below 5 Hz).

2. Sensorless Flux-Vector Control (SVC) provides more precise speed control compared to fixed V/Hz, but is still open loop (no shaft speed encoder). The stator current can be measured and is the vector sum of the flux producing current and the torque producing current inside the motor, which cannot be measured or controlled separately. The vector control must calculate these individual current vectors for all speed and load conditions. For adequate dynamic response the calculations need to be performed thousands of times per second. SVC is typically used for applications requiring higher dynamic performance or operation at low speeds since the speed holding capability is improved compared to fixed ratio V/Hz.

The MVR impeller itself is shaped similar to a small Francis type hydro-turbine runner (see Fig. 2). The overall diameter is approximately 2 m with an inlet diameter of approximately 750 mm and hub height of approximately 500 mm. The impeller was entirely fabricated from 2205 and 2101 duplex stainless steel plate by TIG and MIG welding. The front ring of the impeller varies in thickness from 10 to 25 mm, the back plate is 8–12 mm thick, and the blades are fabricated from 6 mm thick plate. Weld filler metal was 2205. There are 16 full blades, some of which are visible in Fig. 2 and 16 mid-blades, which are positioned in between each of the full blades. The impeller was dynamically balanced at the factory and field balanced after installation.

Just prior to failure, the recorded speed was approximately 1950 rpm, or 91% of the maximum speed of 2150 rpm. Catastrophic failure occurred when the impeller threw a mid-blade during commissioning mode, having run for approximately 150 h. A significant imbalance to the impeller resulted in vibrations that induced the impeller to be shut down. Figs. 2 and 3 show the damaged impeller and thrown blade, respectively.

In this particular case, failure occurred so rapidly and pressure for a return to production was so intense that a root cause failure analysis (e.g., [1]) was undertaken. This was a complex failure with several possible causes that needed to be inves-

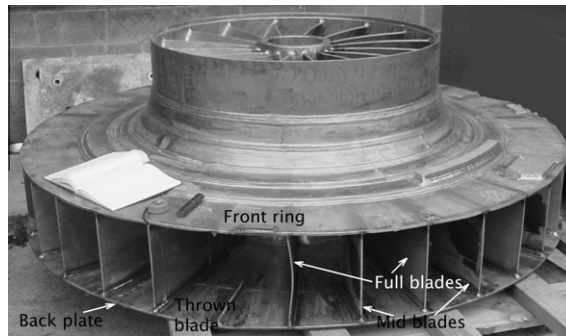


Fig. 2. Failed impeller.

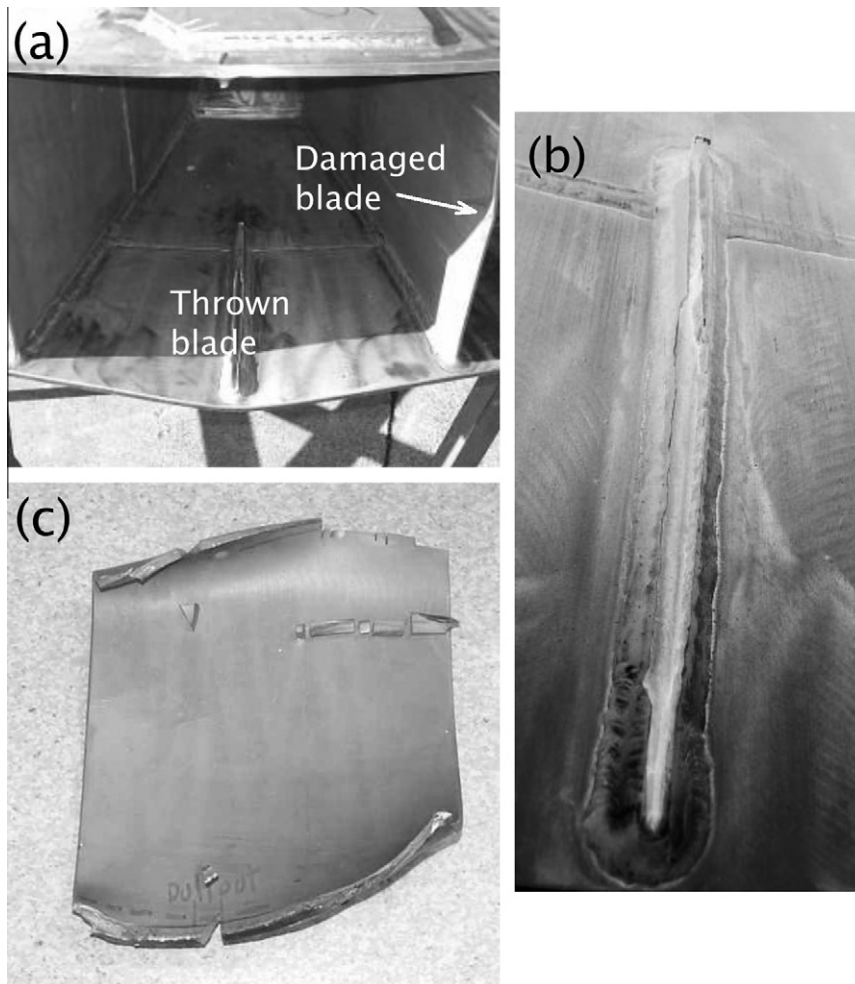


Fig. 3. (a) Original location of the thrown mid-blade and (b) a closer view indicating that there was incomplete fusion on the back plate weld. In (c), the thrown mid-blade is shown as cross-sectioned for subsequent analysis.

tigated by a multi-disciplinary team including a project engineer, a design engineer, a metallurgist and two vibrations specialists.

Analyses of failed MVR impellers are very sparse in the literature [2]. Fatigue failures involving torsional vibrations usually involve shafts, such as crankshafts and drilling equipment (e.g., [3]), rather than the equipment attached to the shafts. In general, rotating equipment should operate with much lower dynamic torque than reciprocating machinery [4]. However, VSD motors have been shown (e.g., [5]) to cause high torsional vibration in fan systems.

The present paper describes the root cause analysis to help reduce the incidences of failures in similar situations. It is important to note that the exact sequence of events was more complicated than is presented here, and that specifics about the application and the component manufacturers are deliberately not revealed.

2. Visual examination and fractography

Visual examination of the failed MVR impeller indicated that there was a lack of fusion in the thrown mid-blade back plate weld, since the plate had simply pulled out of the weld with little adherence evident. Damage to the adjacent blade shown in Fig. 3 indicates the likely sequence of events:

- (1) mid-blade pulled out of the back plate weld;
- (2) the mid-blade fractured by fatigue along the length of the front ring weld;
- (3) the mid-blade was thrown into the adjacent blade denting it as the mid-blade passed out of the impeller.

Visual examination and dye penetrant testing revealed crack indications in almost every blade weld (see Fig. 4). Cracks that led to the edge of blades were yawning, which indicates that residual tensile stress was present. A cracked blade was cut away from the impeller and the crack was opened up for examination (Fig. 5). Beach marks were visual indications of fatigue and numerous initiation sites could be seen on either side of the blade. Scanning electron microscopy revealed the presence of fatigue striations on the thrown blade, which is clear evidence that high cycle fatigue was the cracking mechanism.

3. Metallography

Metallographic samples were ground and polished by standard methods and etched with boiling Murikami's reagent. The microstructure of the blade base plate is normal for 2101 duplex stainless steel plate. Cracks were shown to initiate at the toe of the weld metal in the vicinity of the blade base plate heat-affected zone (Fig. 6). In the heat-affected zone, cracks follow ferrite grain boundaries, which appear to exhibit fine carbide or sigma phase particles (Fig. 7). There was no reason to suspect that the root cause of the failure was metallurgical.

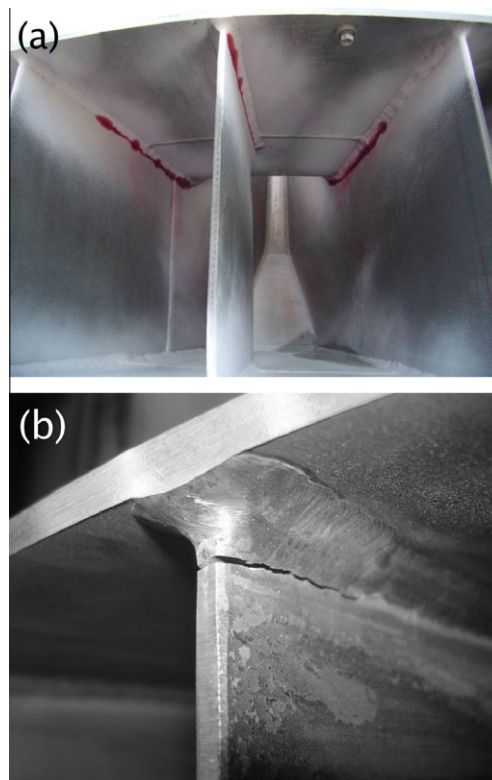


Fig. 4. (a) Numerous crack indications were found on almost every blade. (b) Cracks leading to edges of blades were yawning.

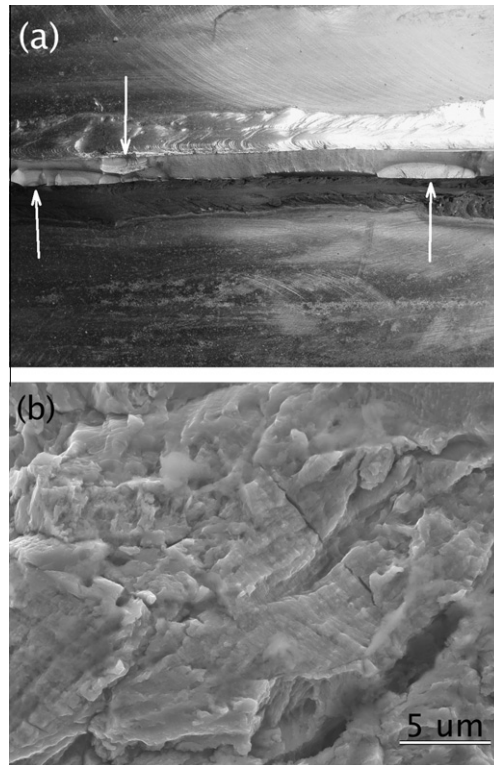


Fig. 5. (a) Opened cracks showed the classic visual appearance of fatigue with many initiation sites on either side of the blade indicated by arrows and (b) Scanning electron microscopy showed fatigue striations on the thrown mid-blade fracture surface.

4. Blade vibration

At this point in the analysis, it was only clear that fatigue was the fracture mechanism and that there was a lack of fusion in the thrown blade. However, other fan blades were cracked as well. One possible explanation for the impeller failure was that the blade with a defective weld fatigued due to resonance, then severe vibrations occurred due to imbalance after the blade was thrown, which in turn resulted in other cracks being formed. The root cause analysis needed to be continued since a source of stress to drive fatigue crack growth in the thrown blade had not been identified.

In seeking a source of stress, two vibration modes were conceptually identified: a blade ‘flapping’ mode and a torsional mode (see Fig. 8). Thus, the first step was to calculate and measure the natural frequencies for structural modes of vibration of the blades, and the torsional frequency for the impeller (front ring relative to back plate). In addition, an impulse response procedure was used to confirm the calculated values. Initial calculations indicated the three lowest “flapping” modes were 438, 567 and 1037 Hz. These compared well with the measured modes of 422, 586 and 1055 Hz respectively. The torsional mode for the whole impeller was calculated approximately as 71 Hz. The impulse response tests using accelerometers glued to the blade surfaces indicated 94 Hz. Note that the impact tests were performed on a damaged impeller with cracked blades, lying with its back plate on the ground. It is likely these issues will have affected the results.

A resonant response of impeller blades, the blade ‘flapping’ mode can cause fatigue failure when one or more of the blade natural frequencies is excited by a disturbing frequency. Such excitation could come from a once-per-revolution impulse as the blade passes the scroll cut-off, i.e., the section that separates the volume of the scroll from the discharge volume.

Since a mid-blade failed and the full blades are stiffer (one would expect higher modal frequencies and thus less likelihood of excitation), calculations were made for mid-blades first. Calculations showed that at the maximum expected impeller speed of 2121 rpm with 32 blades, the passing frequency was 1131 Hz. This means the first three modes of vibration for the mid-blades can be excited by passing the scroll cut-off but the higher modes will not be reached since they occur at speeds beyond the normal operating range. However, inspection on site showed that the scroll cut-off was well rounded and there was a relatively large radial gap of about 120 mm between the impeller periphery and the scroll cut-off. At this point, the concept of blade excitation by coincidence with passing frequency was essentially dismissed.

5. Torsional vibration analysis

Simultaneous with the outcome of the natural frequency calculation exercise, inspection of other MVR system components revealed that the failure was more likely to be torsional. As stated previously, the impeller is one component of an

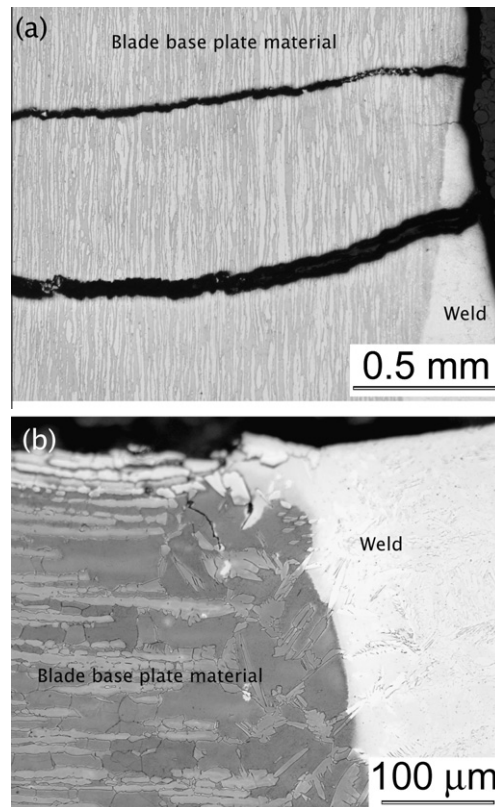


Fig. 6. Metallographic sections of the cracked blades shows that cracks initiate in the vicinity of the toe of the weld metal and the heat-affected zone of the blade base plate.

MVR system, which in turn is only one sub-system of a much larger production system. A schematic drawing of the rotating assembly is shown in Fig. 1. Important components are the motor with a variable speed drive (VSD), which was operating under Sensorless Flux-Vector Control (SVC) at the time of failure. The VSD controls the speed of the motor by varying the frequency and amplitude of the alternating current waveform being delivered to the motor armature [6]. The impeller and motor drive shaft are connected via a pin and coupling with elastomeric bushings, used to minimize effects of mechanical misalignment and to dampen torsional oscillations. The coupling has a stiffness that is variable depending on transmitted torque.

Examination of other components revealed damage to the shaft and coupling bushings. Damaged elastomeric elements are signs of high dynamic torque in the coupling. The shaft exhibited a crack emanating from a keyway oriented at approximately 45° from the shaft surface (Fig. 9), which is typical of failures due to high torsional vibration.

Images of a coupling in place and a cut away to reveal bushings are shown in Fig. 10a. Coupling bushings were heavily worn after service (see Fig. 10b) and were directly observed to be losing material as fine shavings during operation. These two pieces of evidence indicated that there was a significant source of torsional stress that had been unanticipated during design and was previously undetected during operation.

Vibration monitoring is common on rotating machinery to detect mechanical imbalance and bearing condition. In the present case, the transverse and axial components of vibration were monitored continuously and were within the 'normal' range at the time of the failure. However, there was no system to measure torsional vibration. While torsional vibration monitoring is not a normal component of industrial vibration instrumentation, it is important to recognize that mechanical damage to a VSD/motor/driven equipment system [6] may occur because the VSD produces torque harmonics (sometimes called 'torque ripple'), which can result in the development of resonant mechanical responses. Therefore, torsional vibration analysis should be considered in design of such systems [7].

A stroboscope was used to identify the presence of torsional oscillation. While the impeller itself could not be easily observed during operation, oscillatory torsional deflections of the impeller shaft/motor coupling were directly observed by tuning the strobe flash rate to the shaft speed (1700 rpm at the time). These relatively large oscillatory deflections ($\pm 1.5^\circ$) between the two sides of the coupling were observed on close examination of individual frames of a video recording (as shown in Fig. 11a) as a small gap (indicated by an arrow) that is not visible in a subsequent frame (Fig. 11b). The oscillatory torsional deflections indicate that the coupling unloaded during rotation, which is not normal or acceptable for rotating

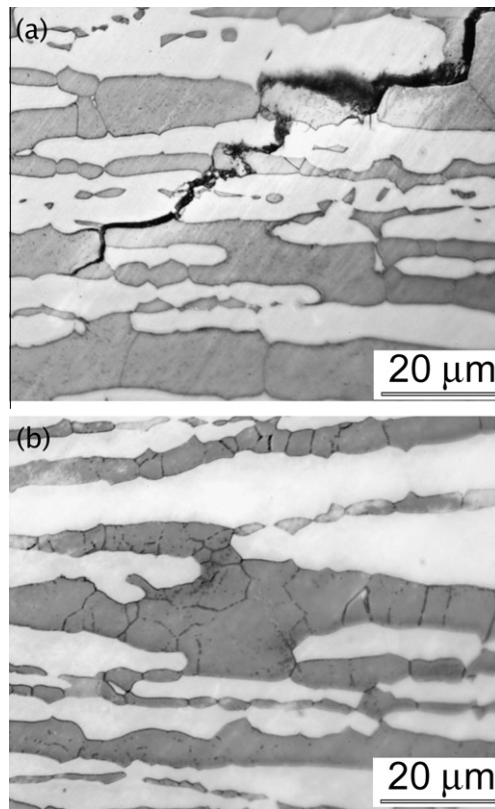


Fig. 7. Cracks preferentially propagate along ferrite (dark phase) grain boundaries and through austenite grains (white). Ferrite grain boundaries may have been embrittled by fine carbide or sigma phase precipitation.

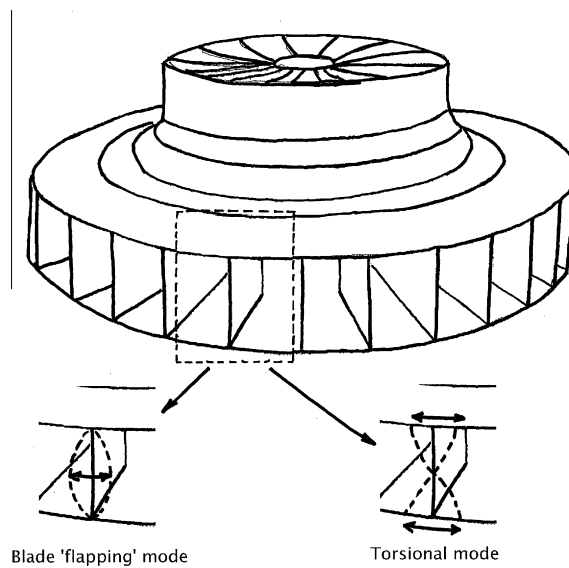


Fig. 8. Possible vibration modes.

machinery. As a general guideline for good reliability of rotating equipment, dynamic torque should remain below approximately 10% of the transmitted torque. This fully reversing torque that occurred during operation would be expected to damage various components of the system.

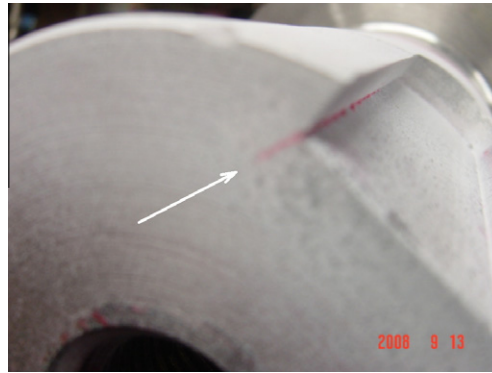


Fig. 9. Impeller shaft keyway with crack revealed by dye penetrant.

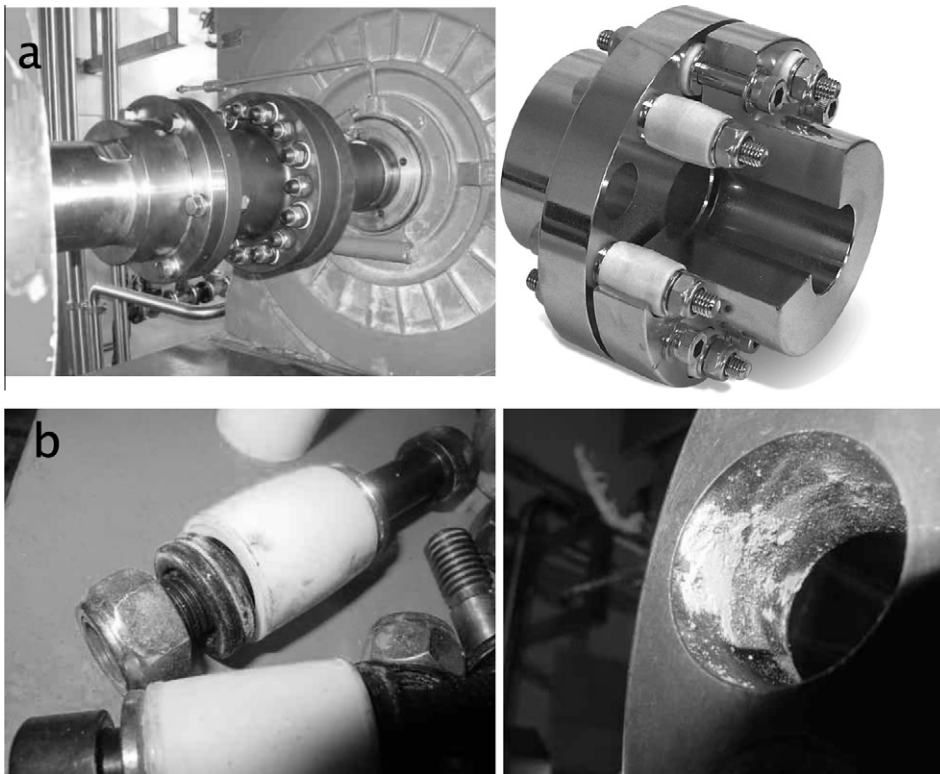


Fig. 10. (a) A shaft coupling in place and a cut-away view showing bushings and (b) worn bushings and wear debris.

In an early field trial, impeller shaft torque data was collected with strain gauges on the shaft adjacent to the coupling, and transmitted via a telemetry system from the rotating shaft to the receiver and logger. Motor current and voltage as well as torque data were recorded on a high-speed waveform recorder. Unfortunately, only 4 s of data was collected at low speed 7.5 Hz (225 rpm) due to fears of further damage to the impeller. It should be noted that 225 rpm is below the normal operating speed range and the fan was running unloaded. In general, the VSD is more stable at higher loads and is (now) set for minimum electrical frequency of 10 Hz (300 rpm fan speed).

At an early stage of the analysis, the Holtzer [8] tabulation method was used to calculate the 1st and 2nd mode torsional natural frequencies (TNF) of the impeller/motor assembly (taking into account the variable stiffness of the coupling) as 9 Hz and 72 Hz at 225 rpm. Fig. 12 shows direct measurements of strain in the shaft with peaks at 11 Hz and 72 Hz, which match the calculated TNFs. The frequency spectrum shown in Fig. 12 is indicative of a coupling at low load that is experiencing backlash (multiple harmonics). Note that the subsequent mass–elastic model (discussed later in this paper) created for

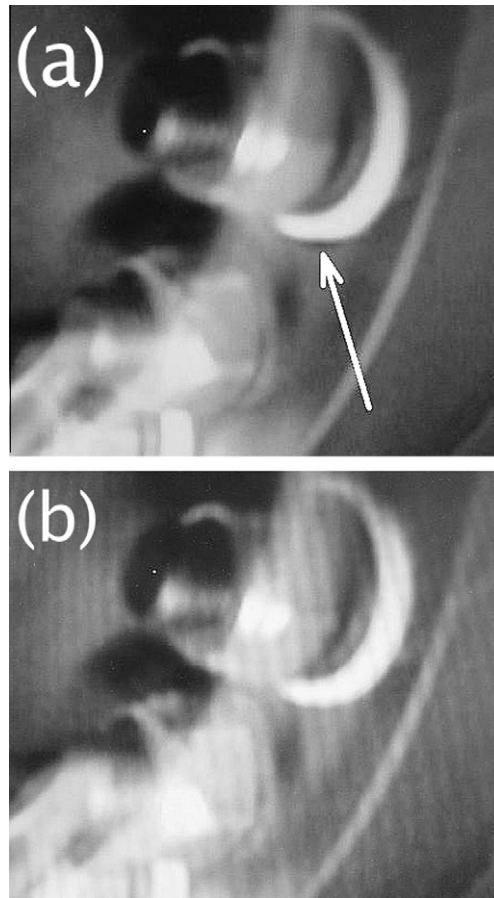


Fig. 11. Two frames from a video recording shows excursions of an elastomer bush. Comparison of the frames shows a gap under the bush in the first frame (indicated by an arrow) not present in the second frame. The gap was measured from the video frames to be approximately 1.7 mm.

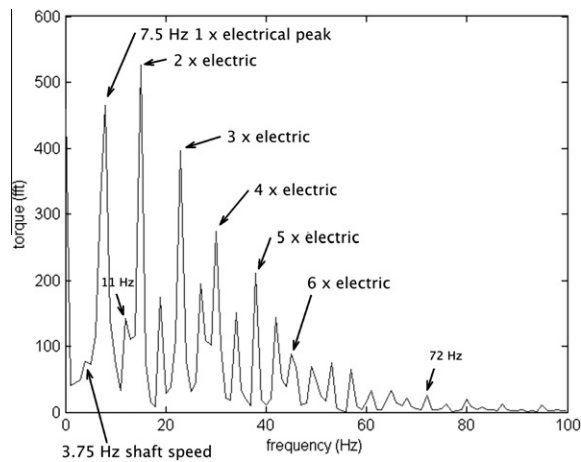


Fig. 12. Fast Fourier Transform plot of torque data for a rotor speed of 225 rpm (3.75 Hz) and controller driving frequency = 7.5 Hz. The shaft was oscillating during this data capture.

the torsional analysis is not valid for this no-load, non-linear condition. At normal operating load and speeds (1000–2115 rpm), the second TNF was measured to be in the 82–88 Hz range (with no cracked blades).

An unexpected result of the strain gauge measurements was the observation that 1st mode oscillations seemed to be present at low levels at all times. These oscillations were excited by plant processes and were sometimes as large as 15% of full power torque.

The strain gauge measurements also showed that, when the system was oscillating severely, the motor controller algorithm produced torque pulses. It is believed that the presence of 1st mode oscillations would trigger this response from the controller. These pulses would be likely to build the amplitude of oscillations in the 2nd mode if left to do so, although only 4 s of data were collected and confirmation of this theory could not be achieved.

Subsequently, a more in-depth analysis used a mass–elastic model to represent the physical system. The rotating masses are represented by a series of lumped inertias connected by equivalent torsional springs, which represent the shaft stiffnesses between the torsional mass inertias. Each significant polar mass moment of inertia was considered in the analysis (e.g., motor rotor, coupling hub, and fan impeller).

Torsional stiffnesses of the shaft sections and coupling were considered when calculating the torsional natural frequencies of a system. The equivalent torsional stiffnesses between lumped inertias were calculated from dimensioned shaft drawings of the motor and fan. Couplings are typically modeled with a torsional inertia at each hub connected by the coupling stiffness. The torsional stiffness of couplings obtained from the manufacturer was used since experience indicates good correlation using their data. It should be noted that the bushing elastic elements have varying torsional stiffness, which is dependent on load and speed. At each speed, the coupling torsional stiffness must be calculated for the transmitted torque.

The torsional natural frequencies and vibration mode shapes were calculated using an eigenvector–eigenvalue matrix solution technique, which directly solves the differential equations of motion for the lumped mathematical model of the torsional system. Normally, the damping in torsional systems is small and has little effect on the natural frequencies. Therefore, the torsional natural frequencies and mode shapes were calculated assuming the damping is zero.

The torsional natural frequencies are determined from the eigenvalues and the mode shapes from the eigenvectors. Using a mass–elastic model with five (5) lumped inertias can theoretically be used to calculate four torsional natural frequencies. However, practically speaking only the first two (2) will be accurate.

For each torsional mode, node crossings (amplitude equal to zero) usually indicate areas with highest stress while anti-nodes (high amplitude) indicate maximum angular oscillation. Based on the calculated mode shapes shown in Fig. 13, the

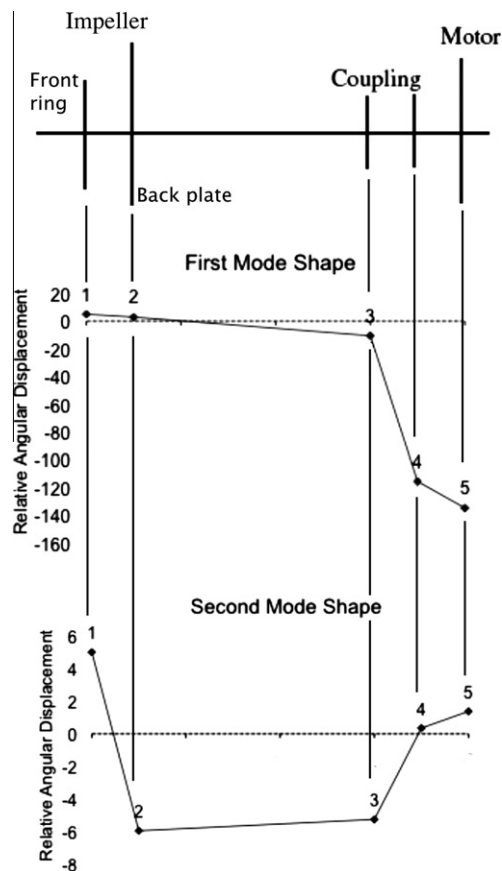


Fig. 13. The first two mode shapes for torsional vibration. These shapes remain relatively constant with coupling stiffness. Note that the scales of the plots are unrelated to each other. Large angular deflections are shown across the coupling in the first mode and across the impeller in the second mode.

first torsional natural frequency would be responsible for causing fatigue cracks in the shaft keyways near the coupling hubs and damaging the coupling rubber elements. The 2nd mode is the one most likely to cause a large oscillatory motion between the impeller front and back plates. The damaging effect of 2nd mode oscillations is by rotating the impeller front ring and back plate to rotate in opposite directions (twisting), which in turn causes large strains at the blade welds.

A Campbell diagram (Fig. 14) is very useful to illustrate the areas of torsional vibration risk in a rotating assembly. The Campbell diagram is obtained by plotting the torsional natural frequencies (open circles and filled diamonds) against the possible sources of excitation, the shaft speed (open squares) and controller frequency (filled triangles). Note that couplings with elastomeric elements introduce more uncertainty into the torsional calculations and can have torsional stiffness values that are $\pm 25\%$ from published catalog values.

There are several issues highlighted by the Campbell diagram:

1. It can be seen that there is a close correspondence between the 1x Electric line (triangles) and the 1st torsional mode line (diamonds) from 0 rpm up to about 800 rpm. This would suggest that any time the controller is induced to act assertively in this rpm range (by a PLC request for example) it will deliver pulses at a frequency that virtually corresponds to the first mode natural frequency. This will excite the 1st mode and potentially drive the system unstable. This seems to be what happened during the data capture at 225 rpm.
2. From 1750 rpm upwards, the 1st TNF mode $\pm 20\%$ (indicating the region for design where natural frequencies should be avoided [9]) overlaps with the 1x Mechanical (i.e., shaft speed) and is at risk of being excited by the shaft rotation alone. This has nothing to do with the controller, but is to do with a low coupling stiffness (a higher coupling stiffness would lift the first mode torsional line clear of the 1x Mechanical line).
3. The 1x Electric line (triangles) overlaps with the 2nd torsional mode from about 1800 rpm onwards. This means that if the controller is induced to act assertively in this range (by a PLC request for example) it will deliver pulses at a frequency that correspond to, and excite the 2nd mode directly. The centre of this range is very close to 2150 rpm, maximum running speed for the impeller.

6. Root cause analysis

A root cause analysis can be clearly summarized by a series of statements, leading backwards from the final failure event to reveal one or more root causes.

1. This analysis was undertaken in response to impeller blades cracking (the final failure event).
2. The impeller blades were cracking due to fatigue.
3. Fatigue was found to be due to reversing torque, i.e., high torsional vibration.
4. An explanation that is consistent with all the data available is that the impeller was damaged by torsional vibrations of the 2nd torsional natural frequency, which was excited by the motor controller algorithm when operating in SVC mode.
5. The fan shaft and coupling were damaged by torsional vibrations of the 1st mode of torsional natural frequency.
6. During the design and specification phase of such equipment it is important that all parties are aware of the possibility of torsional vibrations being induced by the motor and its controller.
7. Likewise, it is important that the system be designed with sufficient separation margins from torsional resonances or shown that operating at or near these resonances will not damage the components. The coupling with rubber elements can be used to provide some damping for the 1st torsional mode; however, the limits of the coupling in terms of allowable dynamic torque and heat buildup must not be exceeded.

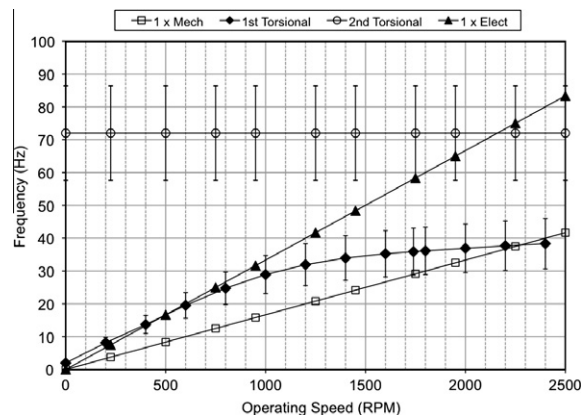


Fig. 14. Campbell diagram. The vertical "error bars" show $\pm 20\%$ the calculated TNFs. Potential resonant condition exists when these bars overlap with the excitation.

8. The present solution to the immediate problem of rapid failure is to use a V/Hz motor controller (open loop), rather than a SVC controller algorithm (with 'virtual feedback'). This avoids significant excitation from the controller and is adequate for the MVR process.

7. Final field test

For long-term service of systems with low damping, it is good practice to avoid having any torsional mode within 20% of the operating speed range [9]. In the present case, the 1st TNF is within this range from 1800 rpm (30 Hz) to the maximum operating speed of 2150 rpm (35.8 Hz). However, for VSD systems with large speed ranges such as the present case, detuning torsional natural frequencies from the operating speed range may not always be practical.

When torsional resonances cannot be avoided, industry specific codes (e.g., API 684 [10]) state that it must be demonstrated (through calculations and/or measurements) that the torsional vibrations will not be damaging to the system. Such a demonstration may be possible if excitation is low (smooth VSD) and/or the damping is sufficient (coupling with rubber elements). Large ID fans used at power plants commonly use couplings with rubber blocks in compression and have the first TNF within the speed range, but are still considered acceptable.

Final field measurements were therefore performed to evaluate the system with Volts/Hertz (V/Hz) configuration. Because the plant was not in production on the day the tests were performed, the machine was free to run at any speed and load. Tests included sweeps of the operating speed range.

The following sensors were used to measure the electrical power, mechanical torque, and fan speed:

Voltage and current probes were located inside the VSD cabinet. Electrical measurements acquired were compared with values from the VSD human interface panel and agreed.

A battery powered strain gage telemetry system was mounted on the fan shaft next to the coupling hub. The output signal from the transmitter was sent to the receiver and then converted to torque. The strain gage telemetry system was initially calibrated using a shunt resistor. The calibration was confirmed once the motor/fan system was running by comparing the mechanical torque from the strain gage telemetry system with the electrical power from the VSD.

A laser tachometer was used to obtain a once-per-revolution pulse on the fan shaft. The rotating shaft speed was determined from this tach signal.

As shown in Fig. 15, the torque and power readings appeared smoother during manual control (fixed speed) compared with automated (power PID) control. For example, PID control increased dynamic torque by 150 N m (zero-peak) compared

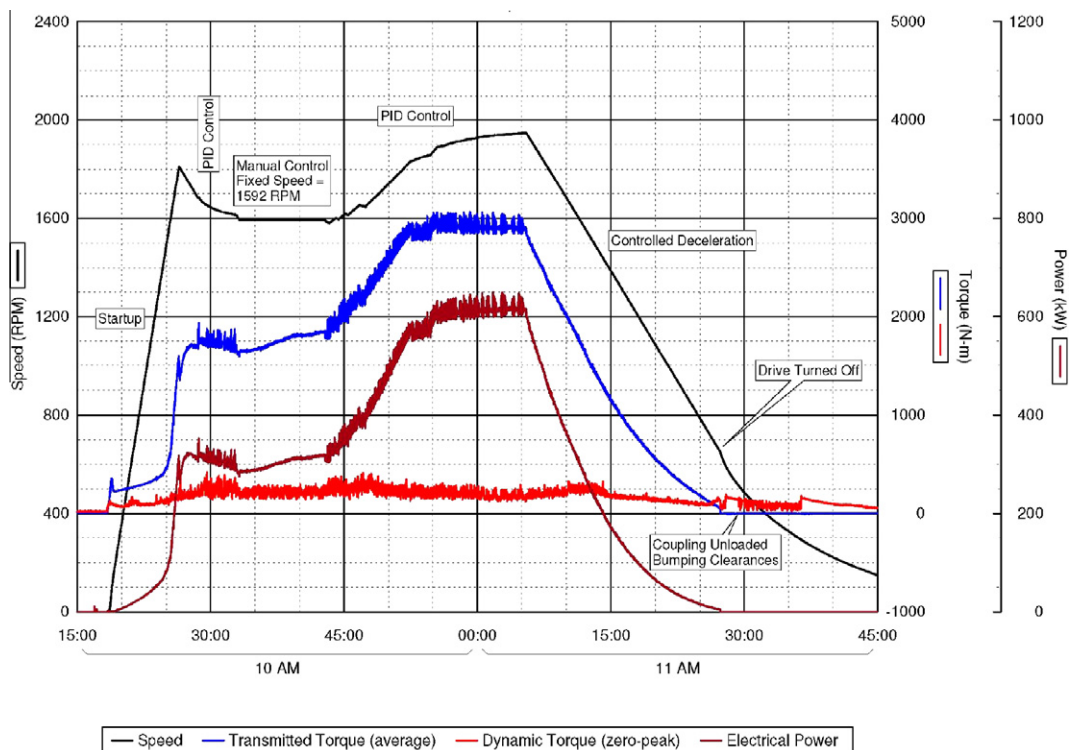


Fig. 15. Final field test measurements of torque in fan shaft.

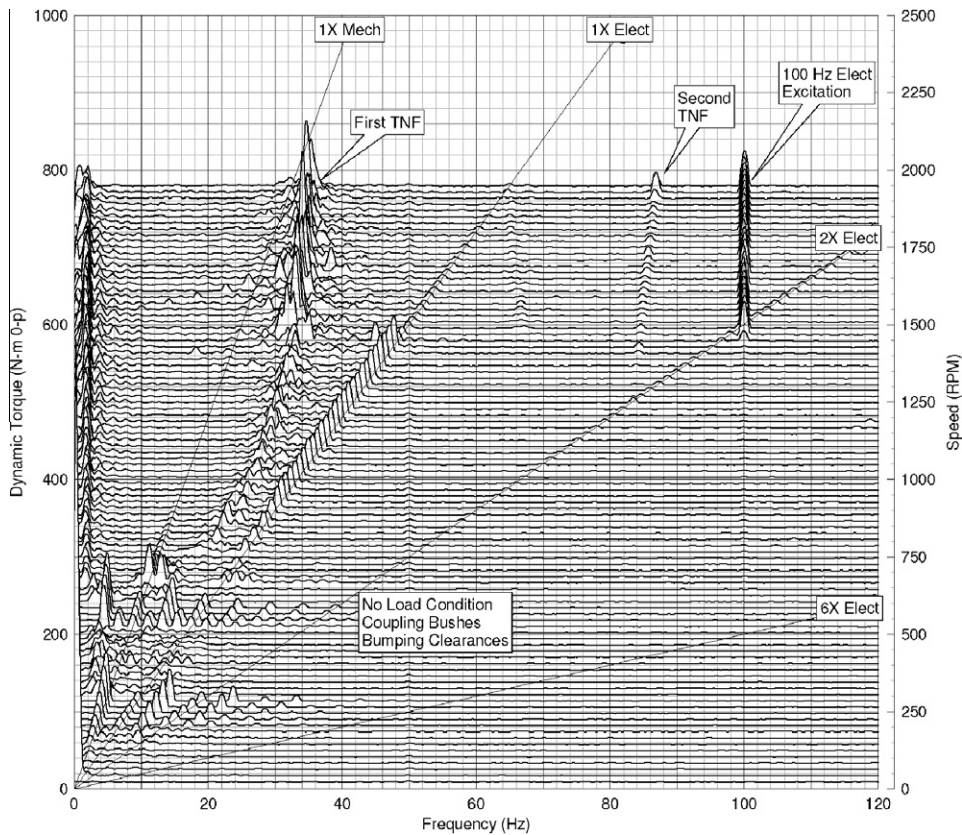


Fig. 16. Waterfall plot taken from torque measurement data.

to fixed speed. In any case, the measured dynamic torque was below 1400 N m throughout the entire speed range, which is considered acceptable for the coupling. In addition, the alternating shear stresses were below estimated endurance limit of the shaft material. Therefore, this level of dynamic torque should not be damaging to the system components.

Waterfall plots were made from the torque measurement to help identify torsional natural frequencies of the system. Fig. 16 shows a waterfall plot of the torque during the powered shutdown. The first TNF, which is associated with twisting through the coupling varied from 20 Hz (at 750 rpm = 12.5 Hz) up to 36 Hz (at the maximum speed of 2115 rpm = 35.25 Hz). The variation in frequency is due to the increased load at higher speeds and the progressive torsional stiffness of the coupling. The second torsional natural frequency of the system, which is associated with twisting through the fan impeller, was found to be approximately 82–88 Hz.

8. Summary and recommendations

Early failure of an MVR impeller was investigated by a root cause analysis. This investigation identified torsional vibration of the impeller/motor system. This vibration resulted in large amplitude twisting between the front ring and back plate of the impeller, large strains at the impeller blade welds and thus fatigue.

The source of the torsional vibrations was found to be the motor controller algorithm operating in Sensorless Flux-Vector Control mode (SVC). The final solution was simply to switch from SVC to V/Hz mode. Exact speed control is not needed in this application, and therefore V/Hz control is an acceptable solution for all parties.

Based on the final measured torsional vibration levels, no additional changes to the motor controller were required. The following recommendations are considered improvements to enhance the operation and should help to minimize the torsional response of the motor/fan system.

1. The motor and fan shafts should have a 2% fillet radius at the base of the keyways to reduce the stress concentration factor from 5 to 3. This is recommended by ASME Standard B17.1 “Keyseats and Keyways”. Square cut keyways have higher stress concentration factor (SCF) than ones with fillet radius [11]. Using an interference fit and eliminating the keyway would further reduce the SCF.

2. The rubber elements in the coupling must be periodically inspected for wear. Historically, excessive wear is indicated by white powder collecting inside the coupling guard. Once the bushes start showing increased wear, they should be replaced as part of the regular maintenance program. Excessive misalignment, high ambient temperatures and/or frequent rapid reversing may necessitate more frequent inspections.
3. As mentioned previously, torsional vibration analysis should be considered part of the design process [7]. In the present case, for example, a different coupling could have changed the torsional characteristics of the mechanical system and may have reduced torsional vibration, regardless of the VSD operating mode.

References

- [1] Mobley RK. Root cause failure analysis. Oxford UK: Butterworth; 1999.
- [2] Kim T-G, Lee H-C. Failure analysis of MVR (machinery vapor recompressor) impeller blade. *Eng Fail Anal* 2003;10(3):307–15.
- [3] Moradi S, Ranjbar K. Experimental and computational failure analysis of drillstrings. *Eng Fail Anal* 2009;16(3):923–33.
- [4] Feese T, Hill C. Prevention of torsional vibration problems in reciprocating machinery. In: Proceedings of the thirty-eighth turbomachinery symposium, college station TX, Turbomachinery Laboratory, Texas A&M University; 2009. p. 213–38.
- [5] Feese T, Maxfield R. Torsional vibration problem with motor/ID fan system due to PWM variable frequency drive. In: Proceedings of the thirty-seventh turbomachinery symposium, college station, Turbomachinery Laboratory, Texas A&M University, Texas; 2008. p. 45–56.
- [6] Walker DN. Torsional vibration of turbomachinery. New York: McGraw-Hill; 2003.
- [7] Shepard DJ. Torsional vibration resulting from adjustable-frequency AC drives. *IEEE Trans Ind Appl* 1988;24(5):812–7.
- [8] Nestorides EJ, editor. A handbook on torsional vibration. Cambridge UK: Cambridge University Press; 1958.
- [9] Mitchell JS. Introduction to machinery analysis and monitoring. Tulsa (OK, USA): Pennwell Books; 1993.
- [10] ANSI/API. API 684 standard paragraphs rotordynamic tutorial: lateral critical speeds, unbalance response, stability, train torsionals, and rotorbalancing ANSI/API; 2005.
- [11] Peterson JE, Pilkey WD, Clark K. Peterson's stress concentration factors. New York: Wiley; 1997.